Yun Luo, Chuanlong Wang, Wenchun Jiang*, Yu Wan, Weiya Zhang and Yu Wang

Effects of Inner Defects on Creep Damage and Crack Initiation for a Brazed Joint

https://doi.org/10.1515/htmp-2017-0098
Received July 7, 2017; accepted December 4, 2017

Abstract: In the brazing process, some brazing defects like semicircular or straight type are generated due to incomplete filling. In this paper, the creep damage and creep crack initiation (CCI) time of Hastelloy C276-BNi2 brazed joint with defects are investigated by a ductility exhaustion damage model. The effects of defect dimension and filler metal thickness are also discussed. The results show that the different defects have different creep damage distributions and CCI times. The maximum creep damage is located at the defect frontier due to the larger stress concentration. With the increase of semicircular defect radius and straight defect length, the CCI time decreases. The creep fracture is inclined to generate in semicircular defect for the smaller defect area ratio, while it is easy to generate in straight defect for the bigger defect area ratio. As the filler metal thickness increases, the CCI time increases. For the thicker filler metal, the creep crack is easy to initiate in semicircular defect.

Keywords: brazed joint, creep damage, crack initiation, defect, finite element

Introduction

The brazed plate–fin heat exchanger (PFHE) is a key component in the nuclear power industry [1]. The fins and plates are brazed together through the fusion of a filler metal pre-located between the fin and plate. The brazing quality is influenced by many factors including brazing temperature [2], filler metal thickness [3], holding time [4] and cooling rate [5], etc. In the brazing process, some defects such as pores or incomplete gap filling are inevitably generated due to the improper brazing technology. On the other hand, the PFHE often operates at elevated temperature approximately 600–650 °C [5]. Figure 1 shows an example of the macrograph of Hastelloy brazed joint with defects due to the incomplete gap filling. At high temperature, stress concentration always occurs in these defects, which leads to creep crack growth and spontaneous failure [6–8].

In PFHE, the creep strain in and around the brazed joint is larger than that in the base metal [9]. It is important to assess the creep behavior of brazed joint with defects to ensure structure integrity. Jiang et al. [10] studied the creep damage and crack initiation in P92-BNi2 brazed joint containing circular notch, and found that the creep crack initiation (CCI) time increases as the notch radius increases. In our previous work, we found that the notch dimension [11], notch position [12] and double notches [13] greatly influence the creep damage and failure lives. Leinenbach and Koster et al. [14, 15] have made a defect assessment on the quasi-static properties of brazed steel joints by experiment and numerical simulation. They found that the defects generally lead to a decrease of the tensile strength, which is strongly dependent on the size and shape of defect. In addition, they also performed a study on the fatigue and cyclic deformation behavior of brazed joints. Compared to the defect-free specimens, the defect-contained specimens have lower strength and fatigue life, and the fatigue strength decreases with the increase of defect size [16, 17]. For brazed specimens, fatigue and residual fracture always occurred in the interface of the brazing zone accompanied by ductile deformation features [18]. Leinenbach et al. [19] also concluded that the fatigue behavior of brazed components is significantly influenced by the interaction of defects and elastic–plastic properties of the substrate material. Morvarid et al. [20, 21] studied the ductile tearing and fatigue crack growth of low carbon steel brazed joint by cohesive zone modeling and found that the higher strain amplitude, the faster the crack propagation along the interlayer. Shi and Yang et al. [22–24] investigated the creep, fatigue life, creep rupture strength and failure mechanism of brazed joints. They found that all the brazed joints fractured at the filler metal and exhibited a lower creep life compared with base metal.

***Corresponding author: Wenchun Jiang,** State Key Laboratory of Heavy Oil Processing, College of Chemical Engineering, China University of Petroleum (East China), Qingdao 266580, PR China, E-mail: jiangwenchun@126.com
Yun Luo: E-mail: luoyun1003@163.com, **Chuanlong Wang:** E-mail: 15763949393@163.com, **Yu Wan:** E-mail: 1563279465@qq.com, **Weiya Zhang:** E-mail: zhangweiya187@163.com, **Yu Wang:** E-mail: 772584055@qq.com, State Key Laboratory of Heavy Oil Processing, College of Chemical Engineering, China University of Petroleum (East China), Qingdao 266580, PR China

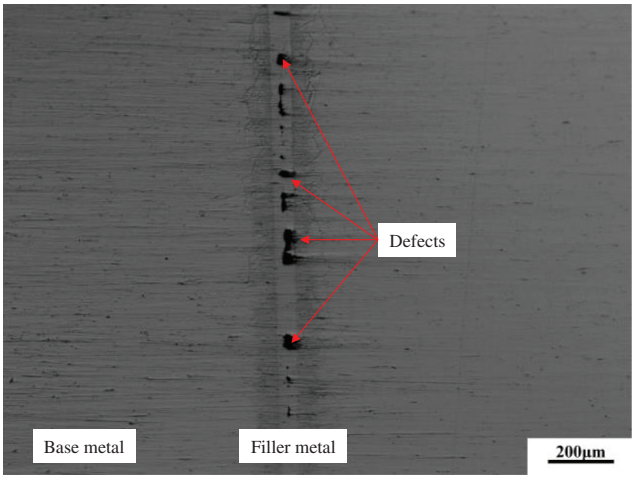

Figure 1: The macrograph of brazed joint containing defects.

Generally, the brazing defects exist in brazed seam due to the incomplete filling or voids. Up to now, it is still unclear how the brazing defects affect the creep behavior of brazed joint, and it is very difficult to investigate the effects of brazing defects on creep damage of brazed joint by experiments The finite-element method (FEM) is an available tool to study creep behavior and has been subjected to more and more application. Thus, the aim of the present work was to study the creep damage behavior of defect-contained brazed joints by FEM. And the defects of type, dimension and filler metal thickness on creep damage, crack initiation and growth have been discussed fully, which will provide a theoretical basis to establish accurate evaluation criteria of brazed structure for high-temperature damage.

Finite-element models and numerical procedures

Material

The material used in this work is a Hastelloy brazed joint by vacuum brazing method. Two Hastelloy C276 plates were brazed together by a nickel-based filler metal BNi-2: the assembly is heated to 600 °C at 10 °C/min and held about 60 min, then it is heated to the brazing temperature 1,050 °C and held about 25 min; at last, the assembly is cooled to the ambient temperature. The creep and elastic–plastic material parameters of the Hastelloy C276 at 600 °C in the literature [13] were used. The Young's modulus E and yield stress of Hastelloy C-276 and BNi-2 at 600°C are 192 GPa, 307 MPa and 173 GPa, 205 MPa, respectively. The isotropic hardening law is employed in the analysis.

In this paper, the creep constitutive equation is assumed to obey the Norton equation:

$$\dot{\varepsilon}_c = \dot{B}\sigma^n \tag{1}$$

where $\dot{\varepsilon}_c$ is the strain rate (s^{-1}); σ is stress (MPa); and B and n are material constants for creep. The creep parameters for base metal and filler metal are listed in Table 1.

Table 1: Creep constants at 600 °C.

Material	B/MPa^{-n}h^{-1}	n	ε_f
Hastelloy C276	1.26×10^{-28}	9.63	0.08
BNi-2	8.75×10^{-40}	14.75	0.0027

Finite-element model

The T-joint specimens were employed in this study. Figure 2 shows the geometry sketching of brazed joint with semicircular defect and straight defect. The filler metal thickness is 100 μm. The radius and length for semicircular and straight defects are 2 and 0.5 mm, respectively. So the defect areas for semicircular and straight defects are 6.3 and 8.0 mm^2, respectively. A three-dimensional (3D) model was created with the FE software ABAQUS 6.10. The finite-element meshing is shown in Figure 3. In the brazing zone, the element size was set to 0.05 mm. The meshing is intensive in brazed seam and then becomes coarse far away. The element

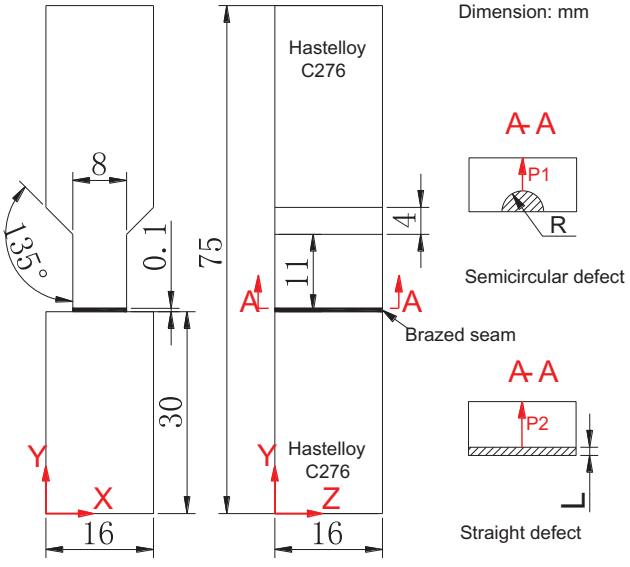

Figure 2: Geometry of brazed joint containing defects.

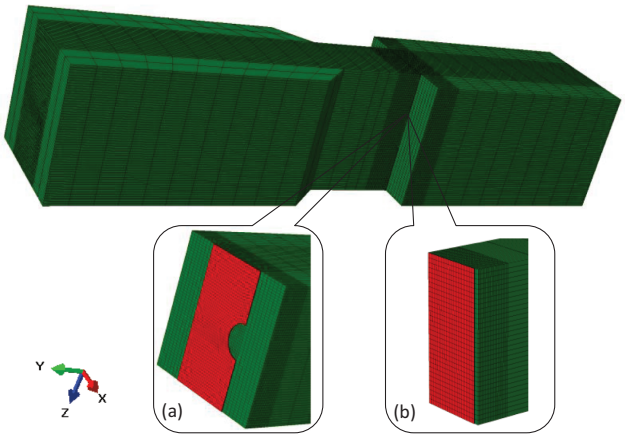

Figure 3: Finite-element meshing for semicircular (a) and straight (b) defects.

type is hexahedral brick elements with 8 nodes (C3D8). The mesh independence on the calculation result has been examined. Table 2 presents the effect of element number on the maximum residual stress in filler metal. It presents that the stress changes little as the element number increases from 84,645 to 143,662. Therefore, the node-element numbers of straight and semicircular defect are 115,688–106,568 and 84,645–78,336, respectively, which can guarantee the calculation precision. In total, a load of 65 MPa is applied. The external load is the same for two type joints. All the nodes on the bottom section were constrained in the *X*, *Y* and *Z* directions.

Table 2: Sensitivity of the element number on the maximum residual stress.

Element number	64,382	84,645	105,428	143,662
Maximum residual stress (MPa)	314	302	302	301

Residual stress calculation

At high-temperature brazing, the assembly is at stress-free state. Therefore, the brazed residual stress is simulated during the cooling from 1,050 °C to 20 °C. The total strain can be decomposed into three components as follows:

$$\varepsilon = \varepsilon^{e} + \varepsilon^{p} + \varepsilon^{ts} \tag{2}$$

where ε^{e}, ε^{p} and ε^{ts} stand for the elastic strain, plastic strain and thermal strain, respectively. Elastic strain is modeled using the isotropic Hooke's law with temperature-dependent Young's modulus and Poisson's ratio. The thermal strain is calculated using the temperature-dependent coefficient of thermal expansion. For the plastic strain, a rate-independent plastic model is employed with von Mises yield surface, temperature-dependent mechanical properties and isotropic hardening model. Temperature-dependent material properties are shown in Figure 4 [13].

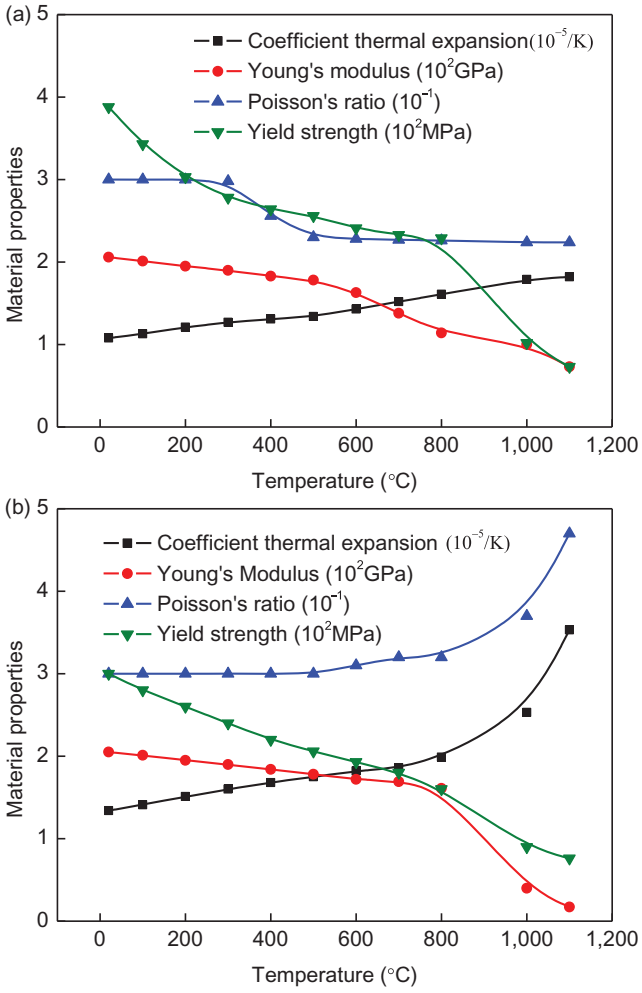

Figure 4: Material properties of Hastelloy C-276 (a) and BNi-2 (b).

Creep damage model

The creep damage accumulation and CCI ahead of a notch are expressed by the ductility exhaustion approach [25]:

$$\omega = \int_0^t \dot{\omega} dt = \int_0^t \frac{\varepsilon_e}{\varepsilon_f^*} dt \tag{3}$$

where ω is the damage varying from 0 to 0.99, and the crack initiation occurs as damage is 0.99. ε_e is the equivalent creep strain, and ε_f^* is the multi-axial creep failure

strain. There are many models to describe the relationship between the creep ductility and stress triaxiality [26]. Here, the Cocks and Ashby model was used which is based on the cavity growth theory by power-law creep [27]:

$$\frac{\varepsilon_f^*}{\varepsilon_f} = \sinh\left[23\left(\frac{n-0.5}{n+0.5}\right)\right] \Big/ \sinh\left[2\left(\frac{n-0.5}{n+0.5}\right)\frac{\sigma_m}{\sigma_{eq}}\right] \quad (4)$$

where σ_m is the hydrostatic stress and ε_f is the uniaxial creep failure strain.

The continuum creep damage model has been incorporated into ABAQUS by a user subroutine CREEP compiled by FORTRAN language. In order to obtain the variables σ_1 and σ_m at each time increment, the USDFLD subroutine has also been embedded into the ABAQUS, and the creep damage is updated at the end of the each increment. The creep constants required in the calculation are shown in Table 3 [28, 29].

Table 3: The summary of simulated results for different defects.

Defect type	Dimension	Area ratio	Axial stress (MPa)	CCI time (h)
Semicircular defect	$R = 2$ mm	0.049	453	26,881
	$R = 4$ mm	0.196	539	1,018
	$R = 6$ mm	0.442	739	84
Straight defect	$L = 0.5$ mm	0.063	380	36,839
	$L = 1.0$ mm	0.125	461	7,289
	$L = 1.5$ mm	0.188	573	865

Results and discussion

Creep and damage distribution

Figure 5 shows the contours of creep damage distribution for the brazed joint with semicircular and straight defects. The location of the maximum creep damage 0.99 represents the position of CCI. Both the semicircular and straight defect joints show that the maximum creep damage locates at the frontier of defect. Typically, for the semicircular defect, the maximum creep damage first emerges in inside and edge of defect, while the maximum creep damage lies in all defects' frontier except for two edges for straight defect. Figure 6 shows the creep damage evolution with time of center point in the filler metal for different defects. The damage first increases quickly then keeps a steady rise rate until 0.99. The damage curve can be divided into two stages: first stage and steady stage. Because the damage (tertiary state) is not considered in creep constitutive model, the tertiary state is not shown in the damage curve of Figure 6. The time when the damage reaches 0.99 is defined as the CCI time. The CCI time for semicircular and straight defect are 26 881 and 38 889 h, respectively. Compared to the straight defect, the semicircular defect is easier to generate creep damage.

According to the damage evolution equation described in the section "Creep damage model," the creep damage is determined by equivalent creep strain (CEEQ) and stress triaxiality. Figure 7 shows the CEEQ and stress triaxiality distribution for semicircular and straight defects. The position of the maximum stress

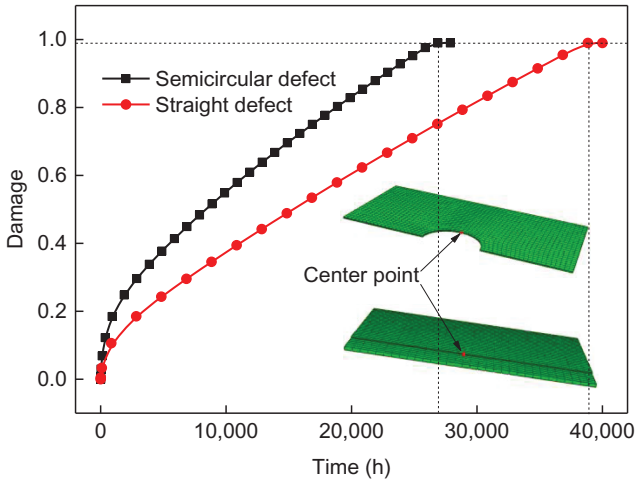

Figure 6: Damage evolution with time of center point in filler metal for different defect types.

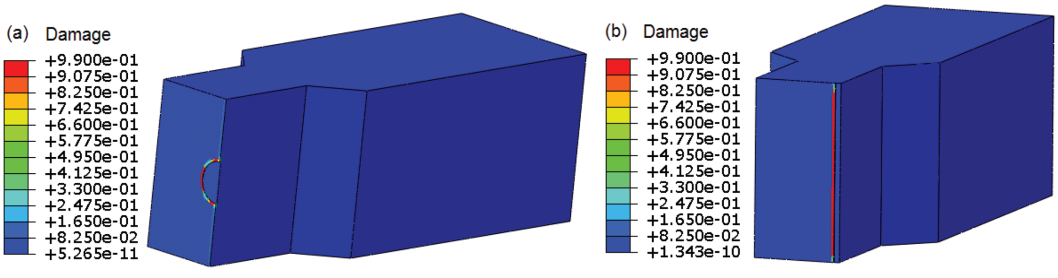

Figure 5: The creep damage distribution for semicircular (a) and straight (b) defects.

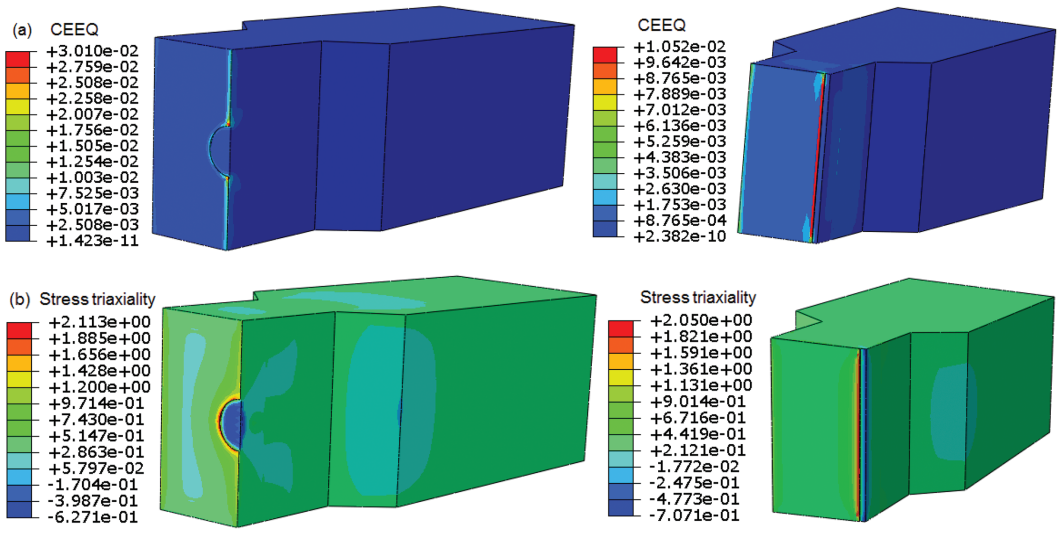

Figure 7: The CEEQ (a) and stress triaxiality (b) distribution for straight and semicircular defects.

triaxility is the same as that of maximum creep damage, while the position of maximum CEEQ is different from that of maximum creep damage. The stress triaxiality plays a more important role in determining creep damage distribution. The maximum CEEQ and stress triaxility for semicircular defect are 0.03 and 2.11, respectively. However, the maximum CEEQ and stress triaxility for straight defect are 0.01 and 2.05, respectively, which are smaller than those of semicircular defect. So the creep damage is easier to generate in brazed joint with semicircular defect.

Different types of defect have a great influence on the creep distribution and CCI time. The different defects may change the stress distribution in filler metal and then lead to the different creep damage behaviors. Figure 8 shows the residual stress and combined stress distribution along P1 and P2. Here, the combined stress is the stress which has been loaded by external load. The stresses along paths P1 and P2 were picked, as shown in Figure 2. Stress components are obtained in the following directions: (1) transverse stress S11 represents the stress in the *X* direction, (2) axial stress S22 represents the stress in the *Y* direction and (3) longitudinal stress S33 represents the stress in the *Z* direction. In Figure 7, the solid point and hollow point represent the residual stress and combined stress distribution, respectively. The transverse and longitudinal residual stresses are almost the same except for some deviations in defect and specimen frontier. The average transverse and longitudinal residual stress are 301 and 302 MPa, respectively. The axial residual stress at interior of brazed seam is very small, even close to zero. After

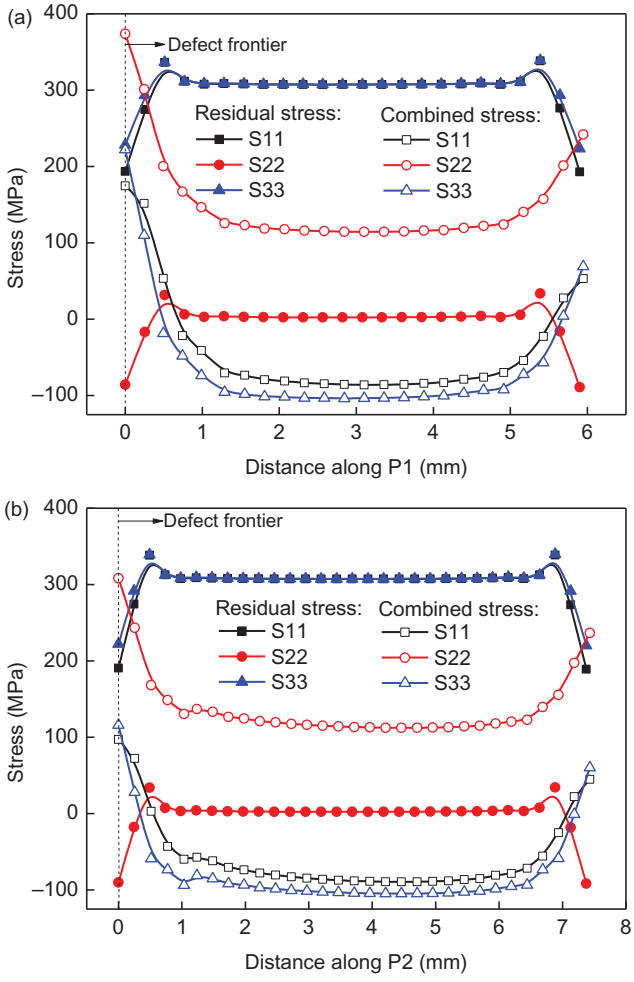

Figure 8: The stress distribution in defect section for semicircular (a) and straight (b) defects.

being loaded by external tension load, both the transverse and longitudinal stresses are decreased while the axial stress is increased. In the interior of the brazed seam, the stress magnitude and distribution of semicircular and straight defect are the same. The average transverse, axial stress and longitudinal stresses of inside seam are −85, 114 and −103 MPa, respectively. However, the stresses at front of defect of three components are all different for two defect types. That is to say, the brazing defects change the stress distribution at the frontier of defect. The transverse, axial and longitudinal stresses at the frontier of straight defect are 97, 308 and 116 MPa, respectively. Nevertheless, for the semicircular defect, the transverse, axial and longitudinal stresses at frontier are 175, 374 and 222 MPa, respectively. The stress in the defect frontier zone for semicircular defect is bigger than that for straight defect. The bigger stress concentrates in the defect frontier zone, the easier the creep damage generates. Thus, the semicircular defect is easy to induce creep damage failure.

Effects of defect dimension

In order to investigate the effects of defect dimension on creep damage, three semicircular defects ($R = 2$, 4 and 6 mm) and three straight defects ($L = 0.5$, 1.5 and 2.0 mm) are discussed in this section. Figure 9 shows the creep damage variation with time for different radii. As the defect radius increases, the CCI time decreases. The CCI time for semicircular defect $R = 2$, 4 and 6 mm is 26,881, 1,018 and 85 h, respectively. The creep failure is inclined to generate for bigger semicircular radius. Figure 10 shows the CEEQ and stress triaxiality variation with time of center point for different defect radii. The CEEQ increases with creep time. For $R = 2$ and 4 mm, the stress triaxiality increases with time, while it increases first then decreases for $R = 6$ mm. At 3,304 h, as the circle radius increases from 2 to 6 mm, the CEEQ and stress triaxiality increase from 0.025 to 0.139 and from 1.791 to 2.859, respectively. At the same creep time, both the CEEQ and stress triaxility of bigger circle radius are bigger than those of smaller circle radius. This is the main reason for the easier initiation of creep crack for bigger circle radius. So the creep damage of bigger circle radius is bigger than that of smaller circle radius before failure. Similarly, the creep damage variations with time of center point for different defect lengths are shown in Figure 11. The CCI time decreases when the straight defect length increases. As the defect length increases from 0.5 to 1.5 mm, the CCI time decreases from 36,839 to 865 h. The deeper the straight defect is, the easier the failure generates. Figure 12 presents the CEEQ and stress triaxiality variation with time of center point for

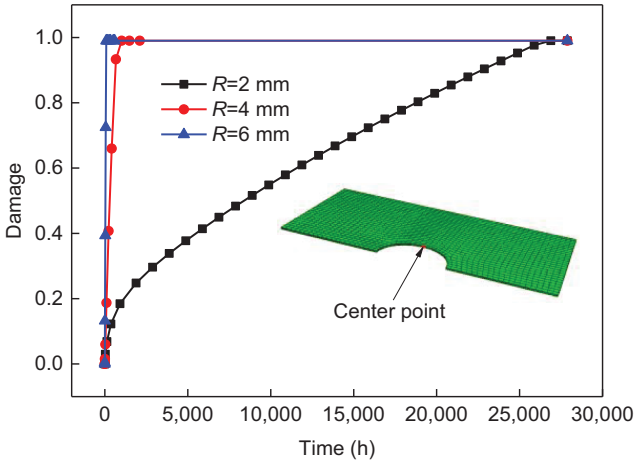

Figure 9: The creep damage variation with time for different defect radii.

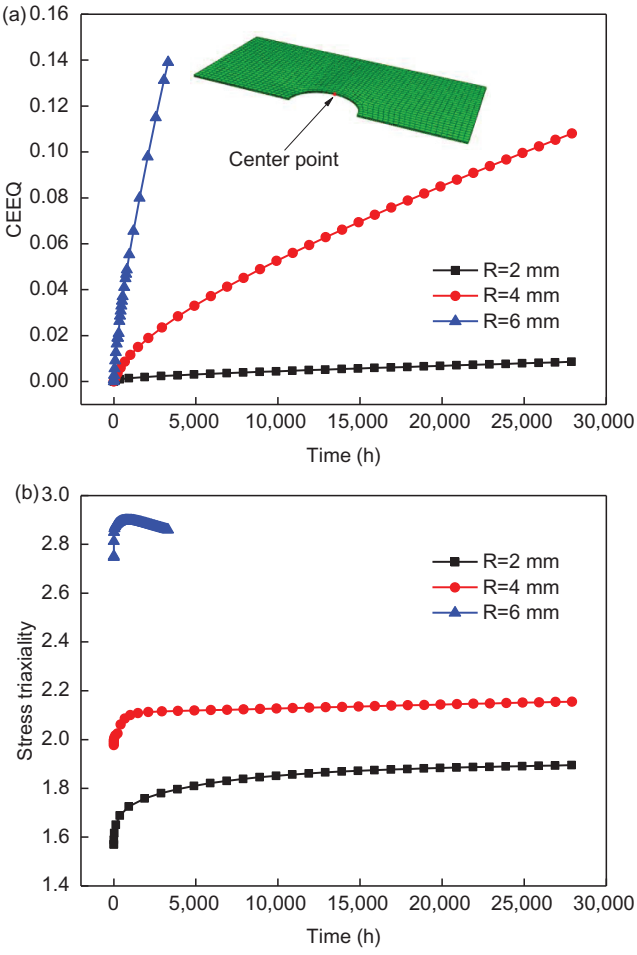

Figure 10: The CEEQ (a) and stress triaxiality (b) variation with time of center point for different defect radii.

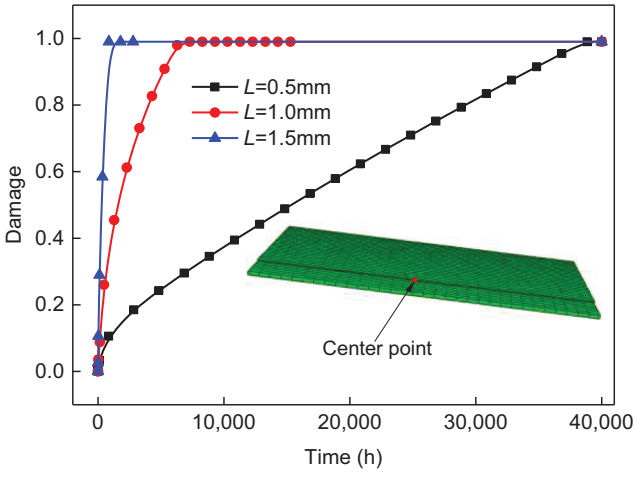

Figure 11: The creep damage variation versus time for different defect lengths.

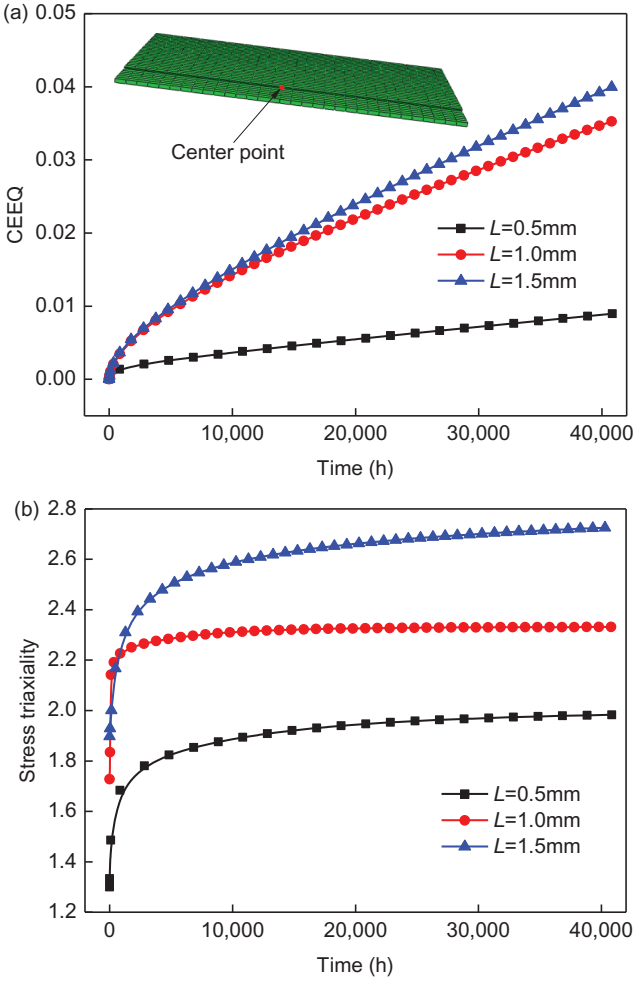

Figure 12: The CEEQ (a) and stress triaxiality (b) variation with time of center point for different defect lengths.

different defect lengths. It shows that both the CEEQ and stress triaxiality increase with time, while the growing rate decreases gradually with time. After 40,800 h, the CEEQ for the defect length from shallow to deep is 0.009, 0.353 and 0.400 and the stress triaxility from shallow to deep is 1.893, 2.331 and 2.726. As the defect length increases, the CEEQ and stress triaxiality all increase. As a result, the creep damage failure is inclined to generate for deep defect length.

Effects of filler metal thickness

As described in [10, 30], the joint thickness plays an important role on the creep damage. The brazed joint thickness should be neither too thick nor too thin [3]. The effects of filler thickness on the creep damage for defect-contained joints should be revealed. Figure 13 shows the effects of filler metal thickness on the CCI time for semicircular defect $R = 6$ mm and straight defect $L = 1.5$ mm. The CCI time increases with the increase of filler metal thickness. As the filler metal thickness increases from 50 to 100 μm, the CCI time for semicircular and straight defect is increased by 74 and 2,447 h, respectively. The increasing rate of CCI time with the increasing of filler metal thickness for straight defect is larger than that for semicircular defect. That is to say, for thicker filler thickness, the creep crack is inclined to initiate in semicircular defect. Compared to thicker filler metal, the CCI is easier to generate in thinner filler metal. As reported by Jiang et al. [9], the creep strain in filler metal is decreased when the filler metal is increased. Therefore, the CCI time is increased, which was also proved by Zhang [30]. But it does not mean that the filler

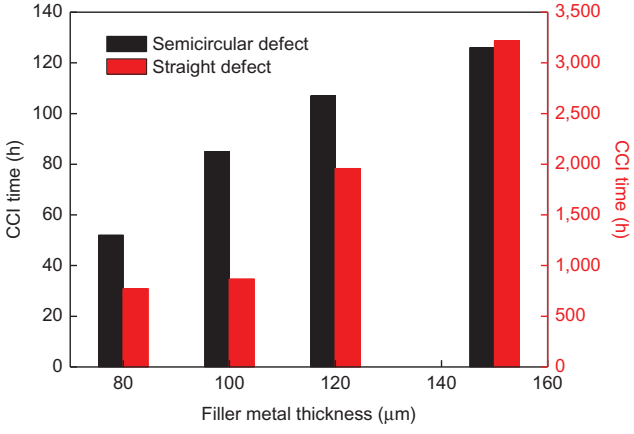

Figure 13: The effect of filler metal thickness on CCI time for different defects.

metal should be as thick as possible. Too thick joint will generate more brittle phases and microcracks in the joint [3], leading to the decrease of mechanical properties of brazed joint. In practice, the filer metal thickness should be enhanced properly under the condition of ensuring good quality of brazing based on site, which is beneficial to improve the service life of the brazed structure.

Discussion

Based on the above analysis, the creep damage distribution and CCI time of filler metal are greatly influenced by the defect type and dimension. As described in the section "Creep and damage distribution," the stress distribution at defect frontier is different for different defects. Especially, the axial stress as a relatively bigger stress has a great effect on the evolution of creep damage. Figure 14 shows the axial stress variation with time at center point for semicircular and straight defects. It obviously shows that the axial stress increases with the increase of defect radius and length even at the creep initial time. At first stage of creep, the axial stress is decreased greatly because of stress relaxation. Then, the decreasing rate becomes smaller until the steady state. At 4,234 h, the axial stresses of center point for $R = 2$, 4 and 6 mm are 356, 449 and 677 MPa, respectively. However, for the straight defect, the axial stress for $L = 0.5$, 1.0 and 1.5 mm are 358, 397 and 468 MPa, respectively. The axial stress distribution in defect (notch) zone has a great influence on the creep damage behavior, which was also proved by Jiang et al. [31, 32]. In the previous study [11, 12], we also proved it. The evolution of axial stress results in the evolution of creep damage, as shown in Figures 8 and 10.

Table 3 summarizes the maximum axial stress in filler metal and CCI time for different defects. The area ratio is defined by the ratio of the size of defect to the size of specimen section. The defect area ratio is decreased as the defect dimension is decreased. For the same defect area ratio, the axial stress and CCI time are different for different defect types. The maximum axial stress increases while the CCI time decreases as the defect area ratio increases for the same defect type. This conclusion is not suitable for different defect types. That is to say, the CCI time will not increase with the increase of defect area ratio for different defect types. For example, the defect area ratio for semicircular defect $R = 2$ mm and straight defect $L = 0.5$ mm are 0.049 and 0.063, respectively. However, the CCI time for $L = 0.5$ mm is smaller than that for $R = 2$ mm. Similarly, the defect area ratios for $R = 4$ mm and $L = 1.5$ mm are 0.196 and 0.188, respectively. But the CCI time for area ratio 0.196 is bigger than that for the area ratio 0.188. Figure 15 shows the variation of CCI time with defect area ratio for semicircular and straight defects. It can

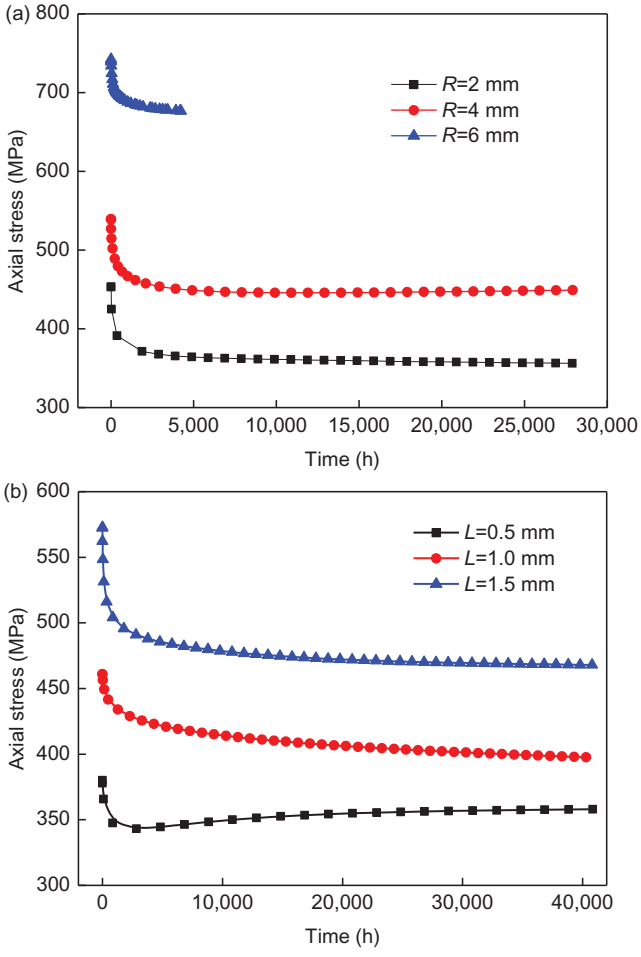

Figure 14: The axial stress variation with time of center point for semicircular (a) and straight (b) defects.

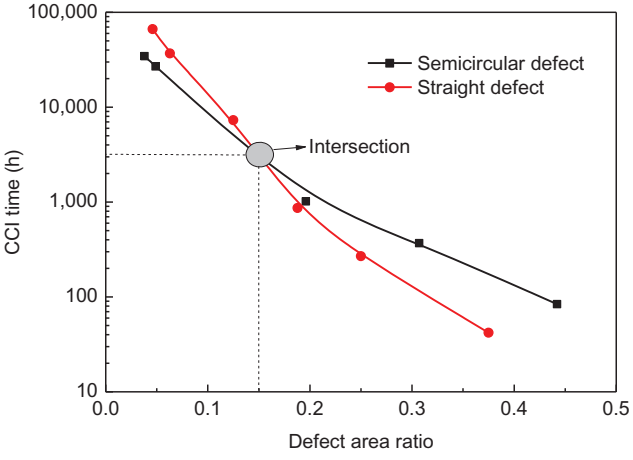

Figure 15: The variation of CCI time with defect area ratio.

be obviously seen that the CCI time decreases as the defect ratio increases. The decrease rate of straight defect is larger than that of semicircular defect. There is an intersection point between semicircular and straight defect. When the defect area ratio is 0.15, the CCI time of semicircular and straight defect are the same. When the defect area ratio is smaller than 0.15, the CCI time of semicircular defect is smaller than that of straight defect. When the defect area ratio is bigger than 0.15, the CCI time of semicircular defect is larger than that of straight defect. Therefore, for the smaller defect area ratio, the maximum creep damage is easy to generate in semicircular defect joints. However, for the bigger defect area ratio, the creep crack is easier to initiate in straight defect joint. Leinenbach et al. [15, 16] found that both the maximal applicable load and quasi-static nominal strength decrease with increase of defect size, which is similar to the conclusion of axial stress found by us. If the defect area ratio exceeds 0.15, both the CCI time of semicircular and straight defect are lesser than 2,000 h. In brazing process, the defect area ratio should be controlled below 0.15 in order to get a longer creep life.

Figure 16 shows the evolution of damage contour with time of filler metal for semicircular defect $R = 6$ mm and straight defect $L = 1.5$ mm. As seen from Figure 16a, the maximum damage initiates at quarter of semicircle away from edge. Then, the creep damage propagates to both sides. And then the maximum damage extends to the inside until fracture. The thumbnail crack specimen is often employed to predict the creep crack growth [33, 34]. Wen [35] also concluded that the creep crack initiates at about quarter of defect, which is the same location of maximum stress triaxiality. As the creep time increases from 84 to 2,002 h, the creep crack length of semicircular defect increases by 2.4 mm. For the straight defect, the maximum damage initiates at the center of defect frontier, as shown in Figure 16b. The creep damage at the defect edge is smaller than that at the defect center. Comparing to semicircular defect, the creep crack growth rate is very slow. As the creep time increases from 864 to 41,792 h, the creep crack length increases by only 0.25 mm. It is again indicated that the creep fracture is easy to generate for semicircular defect because its CCG rate is larger than that for straight defect.

The R6 assessment procedure is generally used for the estimation of defects on the quasistatic loading conditions, which is based on failure assessment diagrams by considering plastic collapse. However, for the changed defect geometries, the R6 procedure [36] may deviate from the experimental results and thus gives a conservative estimation because the specimen geometry is not taken into account [15]. In this study, we have concluded that the brazing defect type and dimension have a great influence on the creep damage behavior and creep fracture time. Therefore, in the defect assessment of brazed structure at high temperature, the effects of defect geometry and size should be fully considered.

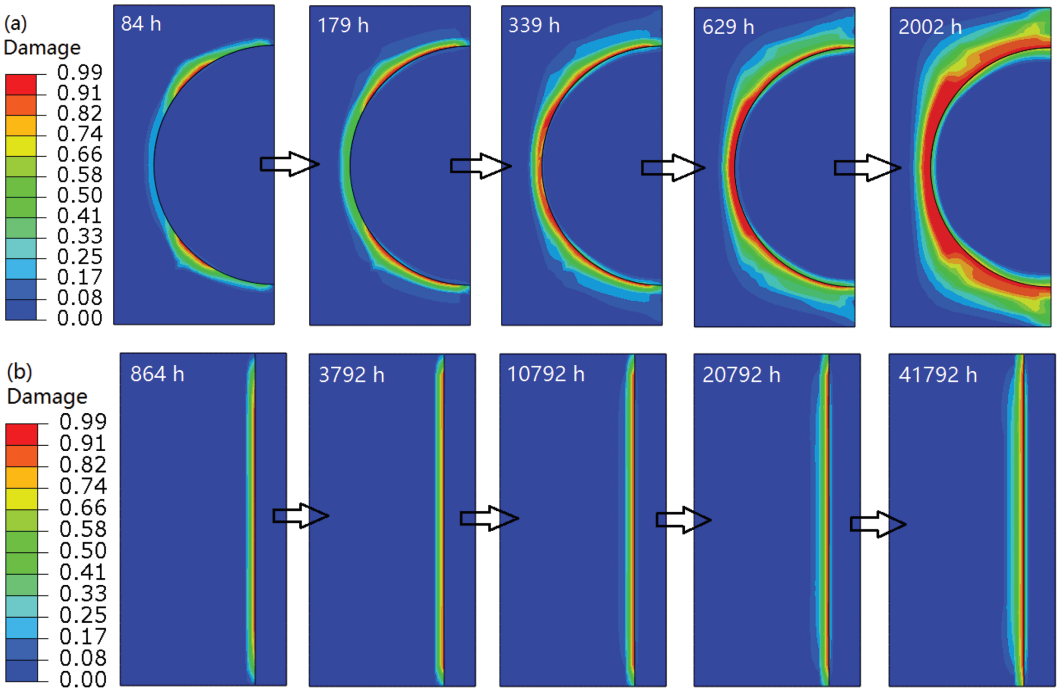

Figure 16: The evolution of damage contour with time of filler metal for semicircular defect $R = 6$ mm (a) and straight defect $L = 1.5$ mm (b).

Conclusions

In this work, the creep damage of Hastelloy brazed joint with semicircular and straight defects are investigated using 3D FEM method based on ductility exhaustion damage model. The following conclusions can be drawn:

(1) The maximum creep damage locates at the defect frontier. Different defect types have different CEEQ and stress triaxiality, which leads to the different creep damage distribution.

(2) The CCI time has an inverse relationship with the axial stress in defect frontier. The bigger the stress concentrated in frontier zone of defect, the easier the creep damage generates. As the semicircular defect radius and straight defect length increase, the CCI time decreases. The creep crack growth rate for semicircular defect is larger than that for straight defect.

(3) For the same defect type, the CCI time decreases as the defect area ratio decreases. The creep fracture is easy to generate in semicircular defect for smaller defect area ratio, while it is easy to generate in straight defect for the bigger defect area ratio.

(4) The CCI time increases as the filler metal thickness increases. The increasing rate of CCI time with filler metal thickness of semicircular defect is smaller than that of straight defect. An appropriate increase of filler metal thickness is beneficial to improve the life of brazing structure.

Funding: The authors gratefully acknowledge the support provided by the Taishan Scholar Foundation (ts201511018), National Natural Science Foundation of China (11372359 and 51575531), the Natural Science Foundation of Shandong Province (2014ZRB01863) and the Fundamental Research Funds for the Central Universities (15CX08006A and 17CX05019).

References

[1] A. Traverso and A.F. Massardo, Appl. Therm. Eng., 25 (2005) 2054–2071.
[2] W. Jiang, J. Gong and S.T. Tu, Mater. Des., 32 (2011) 736–742.
[3] W. Jiang, J. Gong and S.T. Tu, Mater. Des., 31 (2010) 2387–2396.
[4] W. Jiang, J. Gong and S.T. Tu, Mater. Des., 31 (2010) 2157–2162.
[5] W. Jiang, J. Gong and S.T. Tu, Mater. Des., 31 (2010) 648–653.
[6] C. Leinenbach, H.-J. Schindler, T.A. Başer, N. Rüttimann and K. Wegener, Eng. Fail. Anal., 17 (2010) 672–682.
[7] B. Su, Z. Zhou, Z. Wang, Z. Li and X. Shu, Mater. Lett., 136 (2014) 37–40.
[8] J.F. Wen, A. Srivastava, A. Benzerga, S.T. Tu and A. Needleman, J. Mech. Phys. Solids, 108 (2017) 68–84.
[9] W. Jiang, J. Gong, H. Chen and S.T. Tu, Int. J. Pres. Ves. Pip., 85 (2008) 569–574.
[10] W. Jiang, W. Zhang, G. Zhang, Y. Luo, Y.C. Zhang, W. Woo and S.T. Tu, Mater. Des., 72 (2015) 63–71.
[11] Y. Luo, W. Jiang, W. Zhang, Y.C. Zhang, W. Woo and S.T. Tu, Mater. Des., 84 (2015) 212–222.
[12] Y. Luo, W. Jiang, Q. Zhang, W. Zhang, W. Woo, S.T. Tu and M. Hao, Adv. Eng. Softw., 100 (2016) 72–81.
[13] Y. Luo, Q. Zhang, W. Jiang, W. Zhang, S. Xu and M. Hao, Mater. Des., 100 (2016) 271–279.
[14] C. Leinenbach, M. Koster, A. Lis and H.J. Schindler, Weld. J., 91 (2012) 42–48.
[15] A. Lis, M. Koster and C. Leinenbach, Mater. Test., 54 (2012) 605–611.
[16] C. Leinenbach, M. Koster and H.J. Schindler, J. Mater. Eng. Perform., 21 (2012) 739–747.
[17] M. Koster, C. Kenel, W.J. Lee and C. Leinenbach, Proc. Mater. Sci., 3 (2014) 1117–1122.
[18] M. Koster, C. Kenel, A. Stutz, W.J. Lee, A. Lis, C. Affolter and C. Leinenbach, Mater. Sci. Eng. A, 581 (2013) 90–97.
[19] M. Koster, A. Lis, W.J. Lee, C. Kenel and C. Leinenbach, Int. J. Fatigue, 82 (2016) 49–59.
[20] M.K. Ghovanlou, H. Jahed and A. Khajepour, Eng. Fract. Mech., 102 (2013) 156–170.
[21] M.K. Ghovanlou, H. Jahed and A. Khajepour, Eng. Fract. Mech., 120 (2104) 43–59.
[22] D. Shi, C.L. Dong, X. Yang, L. Zhang, J. Hou and Y. Liu, Mater. Sci. Eng. A, 545 (2012) 162–167.
[23] D. Shi, C. Dong, X. Yang, Y. Sun, J. Wang and J. Liu, Mater. Des., 45 (2013) 643–652.
[24] X. Yang, C. Dong, D. Shi and L. Zhang, Mater. Sci. Eng. A, 528 (2011) 7005–7011.
[25] J.F. Wen and S.T. Tu, Eng. Fract. Mech., 123 (2014) 197–210.
[26] J.F. Wen, S.T. Tu, F.F. Xuan, X.W. Zhang and X.L. Gao, J. Mater. Sci. Technol., 32 (2016) 695–794.
[27] A.C.F. Cocks and M.F. Ashby, Met. Sci., 14 (1980) 395–402.
[28] W. Jiang, S. Li, Y. Luo, S. Xu, J. Gong and S.T. Tu, Mater. Sci. Eng. A, 661 (2016) 152–159.
[29] J. Shi, S.D. Tu, J.M. Gong and X. Ling, Mater. Mech. Eng., 29 (2005) 20–24.
[30] Y.C. Zhang and D. Ph Dissertation, School of Mechanical and Power Engineer, East China University of Science and Technology in China, (2016) 78–82.
[31] Y.P. Jiang, W.L. Guo, Z.F. Yue and J. Wang, Mater. Sci. Eng. A, 437 (2006) 340–347.
[32] Y.P. Jiang, W.L. Guo and X.J. Shao, Int. J. Fatigue, 29 (2007) 836–842.
[33] C.J. Hyde, T.H. Hyde, W. Sun and A.A. Becker, Eng. Fract. Mech., 77 (2010) 2385–2402.
[34] S. Liu, G.Z. Wang, S.T. Tu and F.Z. Xuan, Eng. Fract. Mech., 154 (2016) 92–110.
[35] J.F. Wen and D. Ph Dissertation, School of Mechanical and Power Engineer, East China University of Science and Technology in China, (2014) 80–87.
[36] I. Milne, R.A. Ainsworth, A.R. Dowling and A.T. Stewart, Int. J. Pres. Ves. Pip., 32 (1988) 3–104.